Journal of Ceramic Processing Research. Vol. 17, No. 5, pp. 419~425 (2016)

J O U R N A L O F
Ceramic Processing Research

Characteristic study of Ga co-sputtered ZnO layers influenced through substrate heating and post annealing

J.H. Yu[a], T.S. Jeong[a], C.J. Youn[a,*], T.S. Kim[b] and K.J. Hong[c]

[a]*School of Semiconductor and Chemical Engineering, Semiconductor Physics Research Center (SPRC), Chonbuk National University, Jeonju 561-756, South Korea*

[b]*Institute of Educational Development, Kunsan National University, Gunsan 573-701, South Korea*

[c]*Department of Physics, Chosun University, Gwangju 501-759, South Korea*

The co-sputtering of dual ZnO and Ga_2O_3 targets was used to fabricate a Ga-doped *n*-type ZnO layers (ZnO:Ga) layers in this work. The performance ZnO : Ga layers were achieved through the substrate heating of 400 °C (Sub:400) and the rapid-thermal-annealing (RTA) of 500 °C (RTA : 500). RTA : 500 had a low resistivity of 5.29×10^{-4} Ωcm and its transmittance was nearly over 95% in the visible-wavelength region. For X-ray photoelectron spectroscopy (XPS) spectra of the O 1s core level, two characteristic peaks were observed at Sub : 400 and RTA : 500 layers. One is the chemical bonding of Zn-O and another one is caused by the Ga-O bonds consisting Ga_2O_3. Whereas, the core level of the P $2p_{3/2}$ XPS spectra was appeared to three peaks. The first dominant peak located at 1117.9 eV was attributed to Ga_{Zn}, which is caused by a Ga^{3+} ion substituting Zn^{2+} ion in ZnO lattice. The other two low-intense spectra took the form of the metallic Ga and oxide bonding. Furthermore, the XPS result indicates that the crystal quality of RTA : 500 is superior to that of Sub : 400. From the photoluminescence measurement, RTA : 500 showed excellent optical properties due to the formation of the low lattice defect in the layer. These finding indicate that the post annealing process of the ZnO : Ga layers is responsible for the improvement of the layer quality.

Key words: Semiconducting II-VI materials, Characterization, Physical vapor deposition processes, Post annealing.

Introduction

Zinc oxide (ZnO), which is a direct band gap of 3.37 eV at room temperature (RT), is currently an attractive material because of its applicability for blue and ultraviolet (UV) light emitting diode (LED) and detectors [1-3]. It is one of the important transparent-conductive-oxide (TCO) materials, which are used as transparent electrodes in various fields such as solar cells and flat panel display devices, because of having lower toxic than other materials of TCO. To achieve these, TCO is required to be the resistivity below 10^{-4} Ωcm, optical transmission above 80%, and an optical band gap larger than that of 3 eV. Thus, it needs to take a high thermal stability because most device-process procedures consist of a series of heat treatments with temperature reaching above 500 °C. Unfortunately, undoped ZnO itself has a high resistivity due to a low carrier concentration despite using transparent high power electronics with excellent optical properties. It is typically *n*-type conductivity that is caused by residual impurities and defects [4-6]. In order to improve electrical property, the group-III dopants of Al, In, and Ga were injected in ZnO. The Al elements of these dopant materials lead to a high reactivity with oxygen during the layer growth, while the Ga dopant is less reactive and has more resistant oxidation in comparison. Moreover, the resistivity of ZnO doped with Ga trends lower than using other group-III elements. Also, the covalent bond length of Ga-O (1.92 Å) is smaller than that of Zn-O (1.97 Å), which minimizes ZnO lattice deformations even at high Ga concentrations [7, 8]. Because of these reasons, Ga has been used as a dopant material in ZnO for TCO. The growth of the *n*-type Ga-doped ZnO (ZnO : Ga) layers has been achieved by several techniques such as radio frequency (RF) magnetron sputtering, pulsed laser deposition, metal organic chemical vapor deposition (MOCVD), and spray pyrolysis [9-12]. However, the layer-growth method heating the substrate requires high growth temperature [13]. Thus, the post annealing process of the as-grown ZnO : Ga layers needs a longer period of time [14, 15]. Generally, it is well known that the properties of ZnO thin films are strongly affected not only by the deposition conditions but also by the post-annealing conditions [16-18]. Post annealing has a large effect on the crystallinity of ZnO thin films, such as grain size, residual strain and so on, thus, it is also an important method for manipulating the mechanical characteristics of the materials [19].

In this paper, the ZnO:Ga layers were grown on the Al_2O_3 substrate, which were varied to several temperatures, by using the RF magnetron co-sputtering system. The post

*Corresponding author:
Tel : +82-63-270-3651
Fax: +82-63-270-3585
E-mail: cjyoun@chonbuk.ac.kr

annealing on ZnO : Ga layers grown at RT was conducted at several temperatures through the rapid thermal annealing (RTA) method. The characterization of the grown ZnO : Ga layers was investigated by X-ray diffraction (XRD), transmittance, Hall effect, X-ray photoelectron spectroscopy (XPS), and photoluminescence (PL) measurements. Based on these results, the characteristic properties of the layers influenced through substrate heating and post annealing were compared and discussed.

Experimental Procedure

ZnO : Ga layers were grown on the (0001) Al_2O_3 substrate by the co-sputtering method through a commercial RF magnetron sputtering system (Aja International Inc., USA). The base pressure was evacuated to a pressure lower than 1.3×10^{-8} Torr. In order to have a uniform layer of thickness, the rotating speed of the substrate was kept at 40 revolutions per minute during the deposition. ZnO (5N, KURT, USA) and Ga_2O_3 (4N, LST, USA) targets of 2-inch diameter were loaded into the sputtering chamber and they were simultaneously run. The surface of the substrate was cleaned with acetone and ethanol for 5 min and was etched in H_2SO_4 : H_3PO_4 = 3 : 1 for 7 min. Then, it was rinsed in deionized water. The target-substrate distance was set at 10 cm. The loaded target was continuously pre-sputtered for 30 min under a 50 W RF power to remove any surface contamination on the target. When the ZnO : Ga layers grew, the RF power of the ZnO and Ga_2O_3 targets was fixed to 80 and 40 W, which were obtained through experimental repetition respectively. During the ZnO : Ga layer growth, Ar gas for background flows was 50 sccm and the working pressure was set at 4 mTorr. The substrate temperature during the co-sputtering was varied by intervals of 200 ºC, from RT to 600 ºC. The thickness of the layers was about 230 nm by adjusting sputtering time. Then, the ZnO : Ga layers grown at RT were post-annealed by using the RTA system at the temperatures of 200, 300, 400, 500, and 600 ºC for 1 min in N_2 ambient. The crystal structure was analyzed by an XRD measurement. Also, the optical transmission spectra were investigated using a UV visible infrared spectrometer. The Hall effect measurement was conducted by the van der Pauw method. At this time, the grown layer was confirmed to be *n*-type. The XPS analysis was conducted using a VG Scientific spectrometer (ESCA-LAB 210R, UK) with Mg *Kα* x-rays (1253.6 eV). In the XPS spectroscopy, the binding energies were calibrated by taking the carbon C 1s peak (284.6 eV) as a reference. And the PL measurement was performed at RT under excitation by a He-Cd laser (Kimmon, 30 mW).

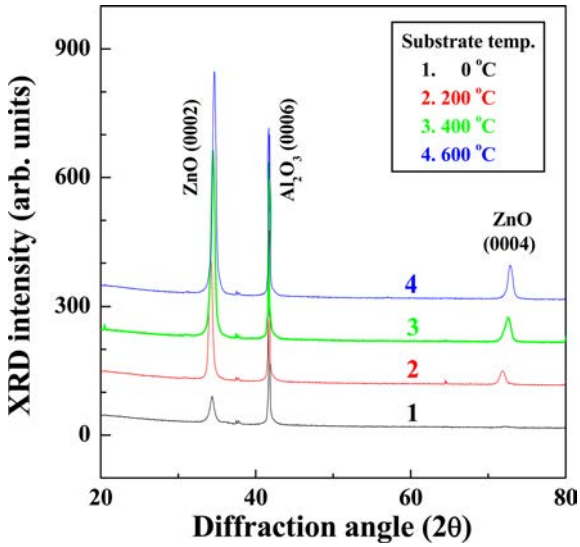

Fig. 1. Rocking curves of the XRD ω-2θ scans on the ZnO : Ga layers grown with the various substrate temperatures. Here, the temperature of 0 ºC means the layer grown at RT.

Results and Discussion

Characteristic behavior of layers based on substrate heating and post annealing

Fig. 1 shows the rocking curves of the XRD ω-2θ scans on the ZnO : Ga layers grown with the variation of the substrate temperature. As shown in Fig. 1, two dominant peaks, except the substrate peak of Al_2O_3 (0006), were observed in each spectrum. These patterns associated with the diffraction peaks corresponding to the (0002) and (0004) phase of ZnO. Except for these peaks, no other peak was observed in the spectrum. This fact indicates that the layers are strongly oriented to the c-axis of hexagonal structure and also crystallized under constraints created by the substrate. With increasing substrate temperature, these spectra tend to have a strong intensity and a narrow full-width-at-half-maximum (FWHM) value. The mean crystallite size of the layers was analyzed by using the Scherrer formula [20]:

Table 1. The structural parameters and band gap energies of ZnO : Ga extracted from the XRD and the transmittance measurements by varying the substrate temperature.

Substrate temperature (ºC)	FWHM (degree)	Lattice constant c (nm)	Biaxial stress (GPa)	Mean crystallite size (nm)	Band gap (eV)
0	0.3370	0.5215	–0.7831	25.18	3.3930
200	0.2728	0.5239	–2.8715	31.10	3.4765
400	0.2711	0.5195	+0.9572	31.32	3.6431
600	0.2689	0.5172	+2.9585	31.59	3.5141

$$D = 0.94\lambda/(B\cos\theta), \quad (1)$$

where λ, θ, and B are the X-ray wavelength (0.15405 nm), the Bragg diffraction angle, and FWHM value on (0002) peak in radians, respectively. Also, the biaxial stress can be calculated from the formula [21]:

$$\sigma = -453 \times 10^9(c\text{-}c_o)/c_o, \quad (2)$$

where c is the measure value of the c-axis lattice parameter and c_o is the strain-free parameter $c_o = 0.5206$ nm. Table 1 listed the structural parameters of ZnO : Ga extracted from the XRD measurement by varying the substrate temperature. As shown in Table 1, the layer grown at 400 °C has a small biaxial stress of + 0.9572 GPa and a mean-crystallite size of about 31 nm. Thus, c-axis lattice parameter is similar to the strain-free parameter of ZnO bulk.

Fig. 2 displays the transmittance spectra on the ZnO : Ga layers grown with the various substrate temperatures. As shown in Fig. 2, the ZnO : Ga layer grown at RT is poor in quality for transmittance and crystallinity. However, the ZnO : Ga layers grown at 200 and 400 °C show the abrupt curvature and an average transmittance of over 90% in the visible-wavelength region. This suggests that high transmittance, due to the reduction of scattering and absorption, leads to high crystal quality. In order to extract the band gap energy from the transmittance result, the model for direct inter-band transitions is generally used as $(\alpha h\nu)^2 = A(h\nu\text{-}E_g)$. Here, A is a function of the refractive index and the hole/electron effective masses, and $h\nu$ is the energy of the incident photon. Also, α and E_g are the absorption coefficients and the band gap energy, respectively. The subfigure in Fig. 2 shows the plot of $(\alpha h\nu)^2$ as a function of photon energy on the ZnO : Ga layers. The E_g can be evaluated from the interception of the extrapolated linear part of the curve with the energy axis. As shown in Table 1, the optical band gap energies were posited from 3.3930 to 3.6431 eV with the temperature variation of the substrate.

Fig. 3 shows the rocking curves of the XRD ω-2θ scans before and after RTA process on the RT-grown ZnO:Ga layers. Here, the RT-grown ZnO : Ga layers were post-annealed by using the RTA method with the temperature variation from 200 to 600 °C for a duration of 1 min in a N_2 atmosphere. As shown in Fig. 3, the peak intensity of

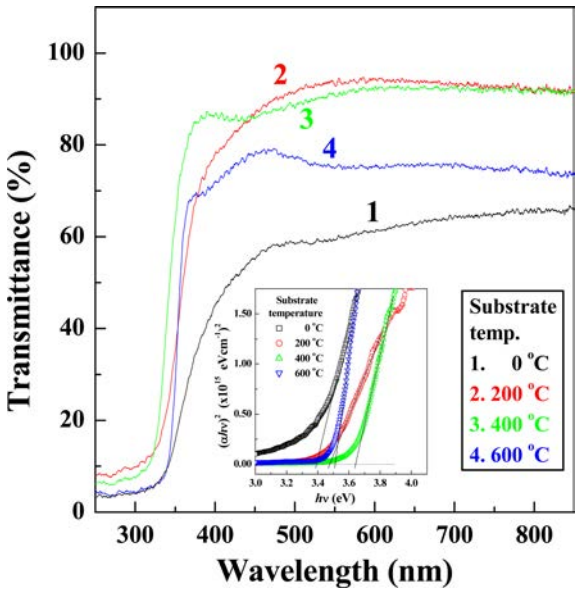

Fig. 2. Transmittance spectra on the ZnO : Ga layers grown with the various substrate temperatures.

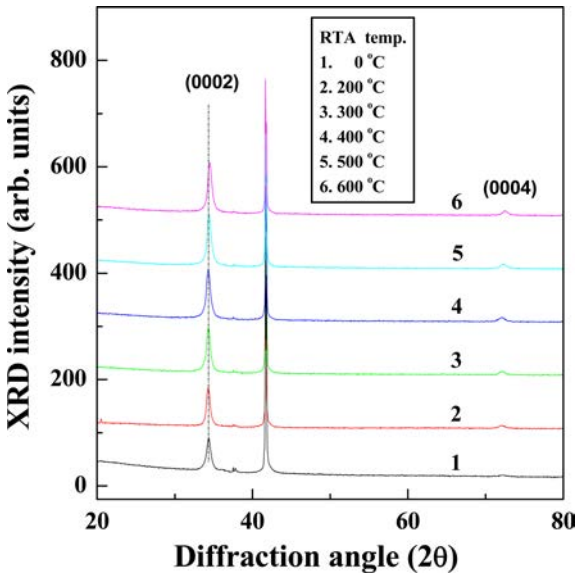

Fig. 3. Rocking curves of the XRD ω-2θ scans before and after RTA process on the RT-grown ZnO : Ga layers.

Table 2. The structural parameters and band gap energies of the RT-grown ZnO : Ga extracted through the XRD and the transmittance measurements by varying the RTA temperature.

RTA temperature (°C)	FWHM (degree)	Lattice constant c (nm)	Biaxial stress (GPa)	Mean crystallite size (nm)	Band gap (eV)
0	0.3370	0.5215	–0.7831	25.18	3.4706
200	0.3188	0.5221	–1.3052	26.62	3.6553
300	0.3172	0.5220	–1.2182	26.76	3.7715
400	0.3078	0.5220	–1.2182	27.57	3.8118
500	0.2983	0.5207	–0.0870	28.46	3.6768
600	0.3052	0.5195	+0.9572	27.82	3.4548

(0002) phase increases until RTA temperatures of 400 °C and then saturated at RTA temperatures over 400 °C. Table 2 summarizes the structural parameters of the RT-grown ZnO : Ga extracted through the XRD measurement by varying the RTA temperature. As Table 2 shows, the crystallite size of the layer shows a tendency of the increase with increasing RTA temperature. At high temperature, the atoms have sufficient diffuse activation energy to occupy the correct site in the crystal lattice and grains with the lower surface energy become larger at high temperature [22, 23]. So, it is believed that the increase of the crystallite size is the merging processes due to RTA. During the growth of the layer, there also include many dangling bonds related to the zinc of oxygen defects at the grain boundaries [24]. Therefore, the RTA process leads to the reduction of the defect centers located in grain boundaries. Consequently, the coalescence into large grains caused by RTA means the improvement of the crystallinity through the post annealing. For the lattice parameter c in Table 1 and 2, ZnO : Ga layers show a small lattice constants when substrate and RTA temperatures are high. This suggests that the Ga atoms due to the high substrate and RTA temperature were acted to the interstitial atoms into the substitutive atoms in the ZnO lattices. This fact is consistent with the result of XPS measurement described below (see Section 3.2.). Most parts of the Ga substituting for Zn make the c-axis shorter, because the ionic radius of Ga is smaller than that of Zn.

Fig. 4 shows the transmittance before and after the RTA process on the RT grown ZnO : Ga layers. As shown in Fig. 4, the curves of the RTA process at low temperatures below 300 °C had a transmittance level below 70%, while, the transmittance curves at RTA temperatures over 300 °C were very transparent with transmittance exceeding 80% indicating good optical quality in the whole visible range. Thus, the curves of the steep gradient clearly indicate the relaxation of the compressive strain remaining in as-grown layers. Increasing the RTA temperature to 500 °C, the transmittance is nearly over 95%, while the transparent degree at RTA temperature of 600 °C was reduced. Therefore, it indicates that excessive RTA process over 600 °C deteriorates the crystal quality of the ZnO : Ga layers. The subfigure in Fig. 4 shows the plot of $(ah\nu)^2$ as a function of photon energy on the ZnO:Ga layers. As shown in Table 2, the optical band gap energy ranges from 3.4548 to 3.8118 eV with varying RTA temperature. The E_g increased with an increasing RTA temperature with a maximum value at the RTA temperature of 400 °C. Thereafter, its decrease was observed. This phenomenon can be explained from the temperature of the RTA process on the ZnO : Ga layers. It suggests that the Ga atoms have been incorporated into the layer caused by the RTA process. If the Ga atoms are located at substitution sites, then there is an increase in the carrier concentration. Consequently, the variation of E_g with increasing RTA

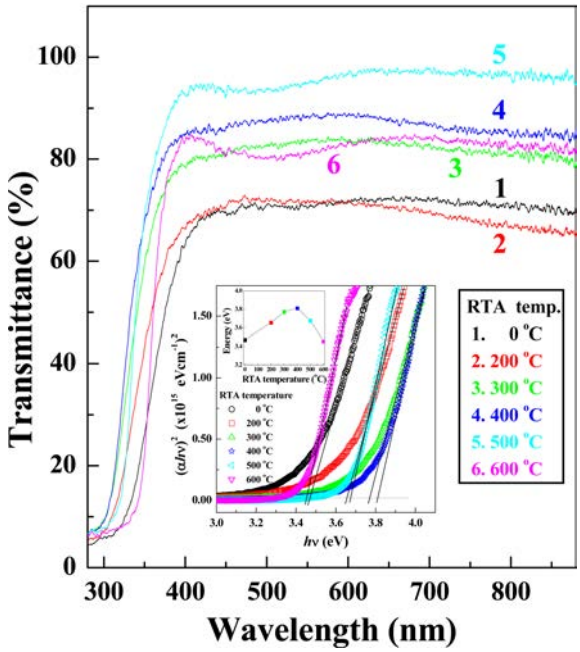

Fig. 4. Transmittance before and after the RTA process on the RT grown ZnO : Ga layers.

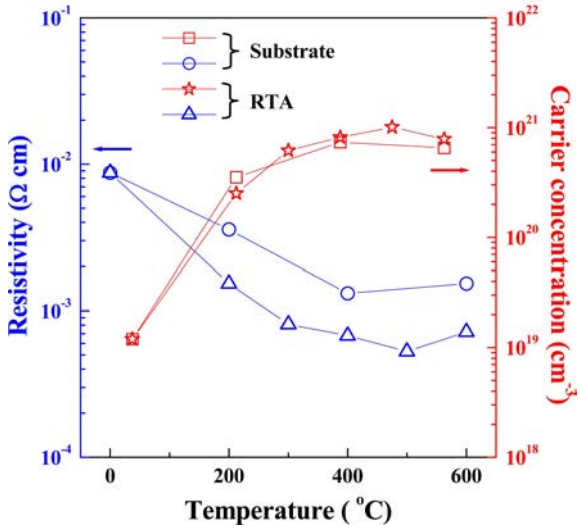

Fig. 5. Resistivity and carrier concentration as a function of the substrate- and RTA-temperature variation.

temperature could attribute to band gap widening due to the Burstein-Moss (BM) effect and band gap narrowing due to many body effects [25]. In the model of BM, the absorption edge shift in an *n*-type semiconductor is dependent on carrier concentration [26,27]. Also, the electronic states in heavily doped and highly excited semiconductors are modified because of carrier-carrier interaction and carrier-impurity interactions. Therefore, many body effects of these interactions lead to a narrowing of the band gap [28].

Fig. 5 shows the resistivity and carrier concentration as a function of the substrate- and RTA-temperature variation. The resistivity measured with the variation of

the substrate temperature was comparatively high in value. Its value was lowest at the temperature of 400 °C, thereafter it was saturated. While the resistivity by RTA process trended toward low value with increasing RTA temperature. Thus, it was about 10^{-4} Ωcm at the temperatures over 300 °C. The lowest temperature of these values was 500 °C and its value was 5.29×10^{-4} Ωcm. From the carrier concentration result, they showed an increase by increasing the substrate and RTA temperatures. The carrier concentration of the specimen annealed at the RTA temperature of 500 °C was observed to be high value of ~ 10^{21} cm^{-3}. However, at the substrate and RTA temperatures over 600 °C, the resistivity was increased and carrier concentration was reduced. It indicates that high substrate-temperature growth and excessive RTA process over 600 °C acts to the cause deteriorating the crystal quality of the ZnO : Ga layers. Judging from these results, it can be estimated that the specimen fabricated under the optimum condition is the layers grown by the substrate temperature of 400 °C (Sub : 400) and processed by the RTA temperature of 500 °C (RTA : 500).

Optical characterization through the XPS and PL observance

In order to find the chemical bond formation on ZnO:Ga layers of Sub : 400 and RTA : 500, XPS measurement was fulfilled after the etching to 5 nm depth from the surface of each specimen. Fig. 6 shows the XPS spectra of O 1s and Ga $2p_{3/2}$ on the specimens of Sub : 400 and RTA : 500. From the O1s spectra shown in Fig. 6(a), the core-level peaks are wide and asymmetric, indicating that at least two kinds of oxygen bond are present. Therefore, these asymmetric peaks can be divided into the two suitable Gaussian components. Then, the O 1s XPS spectrum obtained from Sub : 400 and RTA : 500 layers have two characteristic peaks. As shown in Fig. 6(a), these peaks well coincide with the fitted spectra of I and II. The I peak is known to be located at 530.4 eV and is attributed to O^{2-} ions surrounded by Zn^{2+} ions in the wurtzite ZnO lattice [29]. Therefore, the dominant I peak comes from O-Zn bonds, namely, the chemical bonding of Zn-O [30]. Also, the II peak, which is known to be centered at 531.8 eV, is partially associated to O^{2-} ions present in oxygen deficient regions within the ZnO matrix [30]. Furthermore, the change of the II peak is related to a deviation from stoichiometry in ZnO [31]. Consequently, the II peak suggests being Ga-O bonds. So, it is expected that the chemical formation of the II peak consists of Ga_2O_3 bonds [30]. Thus, this bond could surely be observed in the Ga $2p_{3/2}$ XPS spectrum. As shown in Fig. 6(b), the Ga $2p_{3/2}$ XPS spectra can be also divided by Gaussian fitting. The III peak is attributed to the chemical bonding of Ga-Ga and is located at 1116.8 V. Also, the IV peak found to be 1117.8 eV is associated to the chemical formation caused by a Ga^{3+} ion substituting Zn^{2+} ion in ZnO lattice [32, 33]. These substituted Ga (Ga_{Zn}) atoms at a Zn lattice site behave as a donor. Ordinarily, the Zn vacancy (V_{Zn}) defects in ZnO act as dominant acceptors. However, these V_{Zn} acceptors are compensated by the dominant Ga_{Zn} atoms due to the substituted Ga atoms. Consequently, the ZnO : Ga layers have a *n*-type property. These facts were confirmed through the Hall effect measurement. Then, the low-intense V peak is related to Ga^{3+} in oxide bonding and its chemical bonding consists of Ga_2O_3 [34]. This bonding has the binding energy of 1119.8 eV higher than the value reported of 1118.3 eV [32]. Based on these results, the observation of the metallic Ga and oxide bonding means that only part of Ga atoms is substituted for the Zn lattice site. Table 3 summarizes the binding energy and relative area on each core level of XPS spectra. As Table 3 shows, the relative area ratio of the Ga_{Zn} atoms on RTA : 500 is larger than that

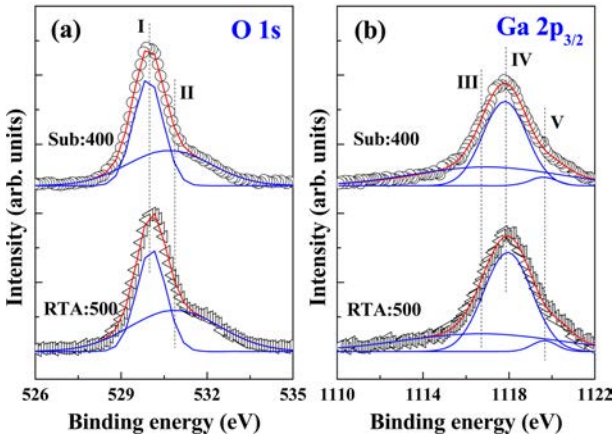

Fig. 6. XPS spectra of O 1s and Ga $2p_{3/2}$ on ZnO : Ga layers of Sub : 400 and RTA:500. Here, (a) and (b) are the core levels of O 1 s and Ga $2p_{3/2}$, respectively. Also, the solid lines in O 1s and Ga $2p_{3/2}$ curves were obtained by using a Gaussian fitting.

Table 3. Binding energy and relative area on each core level of XPS spectra.

Core level	Fitted peak	Sub : 400		RTA : 500	
		Binding energy (eV)	Relative area (%)	Binding energy (eV)	Relative area (%)
O 1s	I	529.9	51.9	530.1	44.8
	II	530.7	48.1	530.9	55.2
Ga $2p_{3/2}$	III	1116.9	40.5	1116.7	35.7
	IV	1117.8	56.0	1117.9	60.9
	V	1119.6	3.5	1119.7	3.4

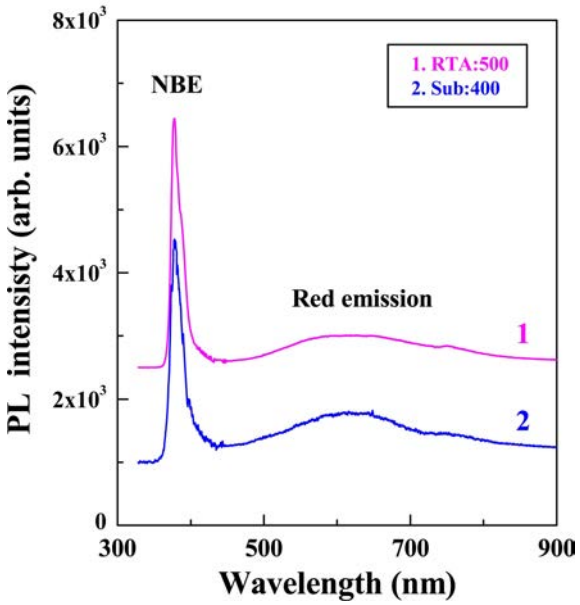

Fig. 7. RT-PL spectra on ZnO : Ga layers of Sub : 400 and RTA : 500.

of the Ga_{Zn} atoms on Sub : 400. It indicates that Ga_{Zn} atoms in RTA : 500 are more abundance than that in Sub : 400. Therefore, abundance of Ga_{Zn} atoms lead to the high carrier concentration in RTA : 500. It consists with the following the result of carrier concentration in Fig. 5.

Fig. 7 displays the RT-PL spectra on ZnO : Ga layers of Sub : 400 and RTA : 500. As shown in Fig 7, a typical PL peaks of ZnO : Ga were commonly observed in the short- and long-wavelength regions of two specimens. The strong UV emission observed at 377.62 nm (3.2833 eV) was associated with the near-band-edge (NBE) emission, which was caused by the free exciton recombination of ZnO [35]. The FWHM values of the NBE emission were 159 and 143 meV at the layers of Sub : 400 and RTA : 500, respectively. The broad red emission centered at 615.82 nm (2.0133 eV) relates to a transition of the excited optical centers from the deep level to the valence band. The origin of this emission is associated with lattice defects in the layers, such as oxygen vacancies (V_O), Zn interstitials (Zn_{int}), and/or these complexes [36, 37]. As Fig. 7 shows, the low intensity of the red emission implies the formation of a low V_O lattice defect in the ZnO : Ga layers because an abundance of V_O ordinarily relates to a stronger intensity of this red emission. Furthermore, the I_{NBE}/I_{red} ratio, the intensity of the red emission being I_{red} and the intensity of the NBE emission being I_{NBE}, is 7.7 for the layer of RTA : 500 and is 4.5 for the layer of Sub : 400. Therefore, the strong intensity and small FWHM of the NBE emission on ZnO : Ga annealed by RTA after the RT growth are positive relation with good crystal quality. So, it suggests that the layer of RTA:500 has excellent optical properties due to the formation of the low lattice defect in the ZnO : Ga layer. Consequently, by comparing the ZnO : Ga layers processed by RTA after the RT growth and grown with varying substrate temperatures, it is found that the optimum RTA process after RT growth can simplify the complicated fabrication procedures and improve the crystalline quality of the ZnO : Ga layers.

Conclusions

The *n*-type ZnO : Ga layers were grown by using the RF magnetron sputtering installed for the dual ZnO and Ga_2O_3 targets. The layer growth was fulfilled according to temperature variation of substrate and RTA. Through the measurement of XRD and transmittance, the layers of Sub : 400 and RTA : 500 among several grown layers showed an excellent crystallinity. The layers of Sub : 400 had a biaxial stress of + 0.9572 GPa and showed an average transmittance of over 90% in the visible-wavelength region. Also, the layers of RTA:500 had a small biaxial stress of –0.087 GPa indicating the strain free and its transmittance was over 95%. Thus, the resistivity of RTA:500 was extracted out to be 5.29×10^{-4} Ωcm. This value was one order of magnitude lower than that of Sub : 400. From the XPS results, the O 1s XPS spectra of Sub : 400 and RTA : 500 layers had two characteristic peaks. One is the chemical bonding of Zn-O and another one is the chemical bonding of Ga-O bonds consisting Ga_2O_3 bonds. For the Ga $2p_{3/2}$ XPS spectra, three other peaks appeared in the Sub : 400 and RTA : 500 layers. Most dominant spectrum of the IV peak is the chemical formation of Ga_{Zn} caused by a Ga^{3+} ion substituting Zn^{2+} ion in ZnO lattice. The two spectra of the III and V peaks took the form of the metallic Ga and oxide bonding. However, the observation of the metallic Ga and oxide bonding means that only part of Ga atoms is substituted for the Zn lattice site. Then, the relative area ratio of the Ga_{Zn} atoms on RTA : 500 was larger than that of the Ga_{Zn} atoms on Sub : 400. Abundance of Ga_{Zn} atoms leads to the high carrier concentration in RTA : 500. So, it suggests that the low resistivity of RTA : 500 is caused by abundance of Ga_{Zn} atoms in ZnO : Ga layers. From the RT-PL measurement, the I_{NBE}/I_{red} ratio for the layer of RTA : 500 is 7.7 and is much larger than the 4.5 for the layer of Sub : 400. Also, the NBE emission on ZnO:Ga annealed by RTA after the RT growth had the strong intensity and small FWHM. These facts indicated that the layer of RTA : 500 had excellent optical properties due to the formation of the low lattice defect in the layer. Therefore, by investigating the characterization of the ZnO : Ga layers processed by RTA after the RT growth and grown with varying substrate temperatures, we knew that the crystal quality of the post-annealed layers after the RT growth is superior to the result of the layers grown by heating substrate. Consequently, these finding indicate that the optimum RTA process after RT growth can simplify the complicated fabrication procedures and improve the crystalline quality of the ZnO : Ga layers for device applications.

Acknowledgments

This research was supported by Basic Science Research Program through the National Research Foundation of Korea (NRF) funded by the Ministry of Education (NRF-2015R1A6A1A04020421).

References

1. S.J. Jiao, Z.Z. Zhang, Y.M. Lu, D.Z. Shen, B. Yao, J.Y. Zhang, B.H. Li, D.X. Zhao, X.W. Fan and Z.K. Tang, Appl. Phys. Lett. 88 (2006) 031911-031913.
2. H. Ohta, M. Kamiya, T. Kamiya, M. Hirano and H. Hosono, Thin Solid Films 445 (2003) 317-321.
3. Q. Yang, X. Guo, W. Wang, Y. Zhang, S. Xu, D.H. Lien and Z.L. Wang, ACS Nano 4 (2010) 6285-6291.
4. D.M. Hofmann, A. Hofstaetter, F. Leiter, H. Zhou, F. Henecker, B.M. Meyer, S.B. Orlinskii, J. Shmidt and P. Baranov, Phys. Rev. Lett. 88 (2002) 045504-1-045504-4.
5. A.F. Kohan, G. Ceder, D. Morgan and C.G. Van de Walle, Phys. Rev. B 16 (2000) 15019-15027.
6. A. Janotti and C.G. Van de Walle, Phys. Rev. B 76 (2007) 165202-1-165202-22.
7. C. Kittel, in "Introduction to solid state physics" 5th Eds., (Wiley, New York, 1976).
8. Q.B. Ma, Z.Z. Ye, H.P. He, S.H. Hu, J.R. Wang, L.P. Zhu, Y.Z. Zhang and B.H. Zhao, J. Cryst. Growth 304 (2007) 64-68.
9. D.H. Oh, Y.S. No, S.Y. Kim, W.J. Cho, J.Y. Kim and T.W. Kim, J. Ceram. Process. Res. 12 (2011) 488-491.
10. G.A. Hirata, J. McKittrick, T. Cheeks, J.M. Siqueiros, J.A. Diaz, O. Contreras and O.A. Lopez, Thin Solid Films 288 (1996) 29-31.
11. A. Behrends, A. Wagner, M.A.M. Al-Suleiman, H. Lugauer, M. Strassburg, R. Walter, A. Weimar, A. Waag and A. Bakin, Phys. Staus Solidi A 209 (2012) 708-713.
12. K.T.R. Reddy, T.B.S. Reddy, I. Forbes and R.W. Miles, Surf. Coat. Technol. 151-152 (2002) 110-113.
13. J.H. Kim, B.D. Ahn, C.H. Kim, K.A. Jeon, H.S. Kang and S.Y. Lee, Thin Solid films 516 (2008) 1330-1333.
14. G.J. Fang, D. Li and B.L. Yao, Thin Solid Films 418 (2002) 156-162.
15. X. Yu, J. Ma, F. Ji, Y. Wang, X. Zhang and H. Ma, Thin Solid Films 483 (2005) 296-300.
16. P.F. Yang, H.C. Wen, S.R. Jian, Y.S. Lai, S. Wu and R.S. Chen, Microelectron. Reliab. 48 (2008) 389-394.
17. H. Chen, J. Ding and S. Ma, Phys. E 42 (2010) 1487-1491.
18. J.H. Han, Y.S. No, T.W. Kim, J.Y. Lee, J.Y. Kim and W.K. Choi, Appl. Surf. Sci. 256 (2010) 1920-1924.
19. L.Y. Lin and D.E. Kim, Thin Solid Films 517 (2009) 1690-1700.
20. B.D. Cullity, in "Elements of X-Ray Diffractions" (Addition-Wesley, Massachusetts, 1978).
21. C.V. Ramana, R.J. Smith, O.M. Hussain and C.M. Julien, Mater. Sci. Eng. B 111 (2004) 218-225.
22. S.Y. Hu, Y.C. Lee, J.W. Lee, J.C. Huang, J.L. Shen and W. Water, Appl. Surf. Sci. 254 (2008) 1578-1582.
23. S.H. Lin and J.L. Huang, Surf. Coat. Technol. 185 (2004) 222-227.
24. X. Teng, H. Fan, S. Pan, C. Ye and G. Li, Mater. Lett. 61 (2007) 201-204.
25. J.G. Lu, S. Fujita, T. Kawaharamura, H. Nishinaka, Y. Kamada, T. Ohshima, Z.Z. Ye, Y.J. Zeng, Y.Z. Zhang, L.P. Zhu, H.P. He and B.H. Zhao, J. Appl. Phys. 101 (2007) 083705-1-083705-7.
26. E. Burstein, Phys. Rev. 93 (1954) 632-633.
27. T.S. Moss, Proc. Phys. Soc. Sect. B 67 (1954) 775-782.
28. D. Auvergne, J. Camassel and H. Mathieu, Phys. Rev. B 11 (1975) 2251-2259.
29. C. Lennon, R.B. Tapia, R. Kodama, Y. Chang, S. Sivananthan and M. Deshpande, J. Electron. Mat. 38 (2009) 1568-1573.
30. J.F. Moulder, W.F. Stickle, P.E. Sobol and K.D. Bomben, in "Handbook of X-ray Photoelectron Spectroscopy" 2nd Eds., edited by J. Chastain, (Perking-Elmer Corporation, Eden Prairie, 1992).
31. Chen, X. Wang, Y.H. Yu, Z.L. Pei, X.D. Bai, C. Sun, R.F. Huang and L.S. Wang, Appl. Surf. Sci. 158 (2000) 134-140.
32. Ahn, S. Lee, W.-J. Kim, G.Y. Yeom and W. Lee, Mater. Sci. Semicond. Process. 16 (2013) 1957-1963.
33. F. Mitsugi, Y. Umeda, N. Sakai and T. Ikegami, Thin Solid Films 518 (2010) 6334-6338.
34. C.L. Hinkle, M. Milojevic, B. Brennan, A.M. Sonnet, F.S. Aguirre-Tostado, G.J. Hughes, E.M. Vogel and R.M. Wallace, Appl. Phys. Lett. 94 (2009) 162101-1-162101-3.
35. D.C. Look, G.C. Farlow, P. Reunchan, S. Limpijum-nong, S.B. Zhang and K. Nordlund, Phys. Rev. Lett. 95 (2005) 225502-1-225502-4.
36. Z.Q. Chen, S. Yamamoto, M. Maekawa, A. Kawasuso, X.L. Yuan and T. Sekiguchi, J. Appl. Phys. 94 (2003) 4807-4812.
37. G. Wang, G. Zhang, J.B. Ketterson and R. Gatt, Thin Solid Films 460 (2004) 232-2326.